OPTOELECTRONICS AND ADVANCED MATERIALS – RAPID COMMUNICATIONS Vol. 4, No. 3, March 2010, p. 299 - 304

Structural, optical and dielectric properties of $ZnTiO_3$ ceramics

P. K. JAIN, D. KUMAR, A. KUMAR, D. KAUR*
Functional nano-materials research laboratory, Department of Physics, Indian Institute of Technology Roorkee, Uttrakhand, India

Zinc titanate ($ZnTiO_3$) ceramics were prepared by conventional solid state reaction method using ZnO and TiO_2 in a molar ratio of 1:1. Various parameters were optimized in order to achieve single phase $ZnTiO_3$. Here, the effect of sintering temperature has been investigated. It was found that the sample sintered at 800 ^oC for 12 hour exhibit single hexagonal phase of $ZnTiO_3$. The indirect band gap of samples sintered at different temperature ranging from 700 ^oC to 1000 ^oC was calculated from absorption spectra, which reveals that band gap is minimum for single hexagonal $ZnTiO_3$ phase (2.88 eV) as compared to mixed cubic/hexagonal phase (2.91 eV). The frequency dependent dielectric properties of these samples have been studied using impedance analyzer. The behavior of capacitance, loss tangent (tan δ) and dielectric constant (ε_r) has been studied in the frequency range 1 kHz to 1 MHz. It is observed that the loss tangent and dielectric constant independent at higher frequency range, which is an important property suitable for various applications.

(Received January 26, 2010; accepted March 12, 2010)

Keywords: $ZnTiO_3$, Dielectric constant, Sintering temperature, Band gap

1. Introduction

TiO_2 and ZnO are both wideband semiconductor with excellent properties and extensive application, and have attracted much interest on either single material [1-3] or ZnO-TiO_2 composites [4-6]. ZnO has attracted intensive research effort for its unique properties and versatile applications in transparent electronics, ultraviolet (UV) light emitters, piezoelectric devices, chemical sensors and spin electronics [7-10]. One of the most important characteristics of ZnO is that it has a large exciton binding energy (60 meV), which is significantly larger than other materials commonly used semiconductor for blue green light-emitters devices, such as ZnSe (22meV) and GaN (25 meV) [11]. On the other hand, titanium dioxide (TiO_2) is one of the most important semiconductors with high photocatalytic activity, being non-toxic, stable in aqueous solution, and relatively inexpensive. The excellent photocatalytic property of TiO_2 is due to its wide band gap and long lifetime of photogenerated holes and electrons [12]. The material, however, presents two main drawbacks during the photocatalytic process: (i) the less use of solar spectrum and (ii) the relatively high electron–hole recombination rate. One of efforts to overcome these problems is to dope TiO_2 with other material [13-14]. Thus, it is possible to enhance the activity of TiO_2 photocatalyst by means of ZnO doping. Up to now, some efforts have been done to modify TiO_2 by means of ZnO doping [15-16].

$ZnTiO_3$ is of a perovskite type oxide structure and could be a useful candidate as microwave resonator [17], gas sensor [18] (for ethanol, NO, CO, etc.), microelectronics [19], metal–air barriers [20], and as high performance catalysts [21-22] for the complete oxidation of hydrocarbons or CO and NO reduction [23] and paint pigment [24]. There are three compounds existing in the ZnO–TiO_2 system including α-Zn_2TiO_4 (cubic), Zinc titanate ($ZnTiO_3$, cubic and hexagonal), and $Zn_2Ti_3O_8$ (cubic) [25-26]. Nevertheless, the preparation of pure $ZnTiO_3$ from a mixture of ZnO and TiO_2 with 1:1 has not been successful because the compound decomposes into α-Zn_2TiO_4 and rutile TiO_2 at about 945 ^oC. There are several methods to prepare $ZnTiO_3$ powder including solid state reaction [27], sol–gel [28], etc. In this study, we attempted to synthesize $ZnTiO_3$ powders by conventional solid state reaction which is simpler to operate and uses cheap and easily available oxides as starting materials.

2. Experimental details

The $ZnTiO_3$ powder was prepared by conventional solid state reaction using 99.99% pure ZnO and TiO_2 powder in a molar ratio 1:1 as the starting materials (Loba Chemie, India). The starting materials were ground for 24 h and then calcined at 400 ^0C for 12 h. The calcined powder was reground for 6 h and was then pressed into pellets of 0.75 cm in diameter and 1.15 mm thickness under the pressure of 90 MPa. Then, the pallets were sintered at different temperatures of 700 ^oC, 800 ^oC, 900 ^oC and 1000 ^oC for 12 h. The phase and orientation of bulk $ZnTiO_3$ samples were characterized by X-ray diffractometry (XRD, Bruker AXS D-8 Advance Diffarctometer) using CuK_α (λ=1.5407 Å) radiation. The surface morphology was examined by field emission scanning electron microscopy (FEI Quanta 200F model)). After dissolving the sample into ethanol, absorption spectra have been taken using UV-vis-NIR spectrophotometer (Varian Cary 500) in the wavelength range 200 nm to 500 nm. The frequency dependent

dielectric measurements were done using impedance analyzer from 1 kHz to 1 MHz. A conventional two-probe technique is used for these measurements. Silver paint was applied on both surfaces of the sample.

3. Results and discussion

3.1 Structural characterization

It is generally difficult to synthesize single phase $ZnTiO_3$ due to the presence of both cubic and hexagonal phases at low temperature and the decomposition into Zn_2TiO_4 and TiO_2 (rutile) at high temperature, therefore, several parameters need to be optimized. Fig. 1 shows the XRD patterns of the samples sintered for 12 h at different temperatures varying from 700 ^oC to 1000 ^oC. The sample sintered at 700 $^\circ C$ shows the coexistence of both cubic and hexagonal-phases. While the sample sintered at 800 $^\circ C$ exhibits pure crystalline phase of hexagonal $ZnTiO_3$ without any peaks of cubic-phase, because cubic-phase of $ZnTiO_3$ is unstable at high temperature and transforms into hexagonal phase. Further increases in sintering temperature upto 900 $^\circ C$ several peaks related to cubic Zn_2TiO_4 and rutile TiO_2 along with the hexagonal $ZnTiO_3$ were observed. The reason may be attributed to the fact that at higher temperature decomposition of hexagonal $ZnTiO_3$ into cubic (Zn_2TiO_4) and rutile (TiO_2) starts to appear. At 1000 ^oC sintering temperature, the fraction of hexagonal phase of $ZnTiO_3$ was found to decrease and the phases like Zn_2TiO_4 and TiO_2 becomes dominant.

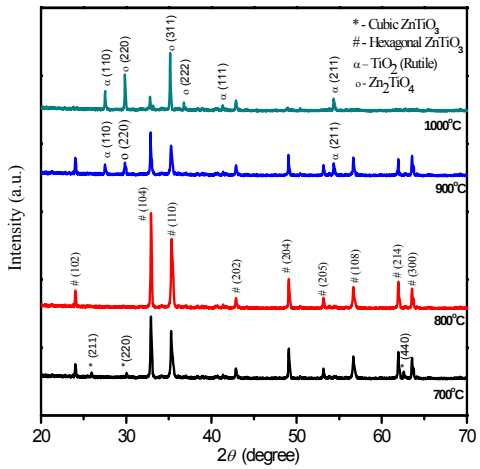

Fig. 1. XRD patterns of ZTO pallets sintered at different temperature.

The crystallite size of these samples were calculated along the (104) orientation of hexagonal $ZnTiO_3$ phase using the following Scherer's formula [29]

$$t = \frac{0.91\,\lambda}{\beta \cos\theta} \qquad (1)$$

where λ= wavelength of x-rays (1.5406Å), β = Full width at half of the maximum peak (FWHM), θ = Bragg's angle. The crystallite size of the samples sintered at various temperature calculated using Scherer's formula are shown in Table 1 and the variation of FWHM and crystallite size are shown in Fig. 2(a).

It is found that the crystallite size increases and FWHM decreases with sintering temperature. According to Ostwald ripening [30], the increase in the particle size is due to the merging of the smaller particles into larger ones and is a result of potential energy difference between small and large particles and can occur through solid state diffusion.

The percentage of hexagonal-phase was estimated approximately from the ratio of areas of hexagonal-phase peaks to the areas of all peaks using the equation as follows:

$$H(\%) = \frac{A_h}{A_{all}} \times 100 \qquad (2)$$

here, A_h and A_{all} denote the areas of hexagonal-phase $ZnTiO_3$ and the areas of all peaks, respectively. The results are summarized in Table 1.

Table 1. Various calculated parameters for different sintering temperature.

Sr. No.	Sintering temperature (°C)	FWHM (β) (degrees)	Crystallite XRD (nm)	Grain size FE-SEM (nm)	Hexagonal-phase (%)
1	700	0.1920	43.14	211	92.47
2	800	0.1470	58.86	248	100
3	900	0.1103	75.10	640	61.19
4	1000	0.1068	80.59	766	05.13

The lattice parameter is calculated using the following formulas:

Cubic:

$$\frac{1}{d^2} = \frac{h^2+k^2+l^2}{a^2} \qquad 3(a)$$

Tetragonal:

$$\frac{1}{d^2} = \frac{h^2}{a^2} + \frac{k^2}{b^2} + \frac{l^2}{c^2} \qquad 3(b)$$

Hexagonal:

$$\frac{1}{d^2} = \frac{4}{3}\left(\frac{h^2+hk+k^2}{a^2}\right) + \frac{l^2}{c^2} \qquad 3(c)$$

where h, k, l are miller indices of crystal planes and d is the spacing between adjacent planes. For a lattice spacing d value, the h, k, l value can be found by comparing with standard data and then by using equation, a, b, c can be calculated. The variation of lattice parameters and

sintering temperature for $ZnTiO_3$ hexagonal phase is shown in Fig. 2 (b).

The increment in lattice parameter and unit cell volume with sintering temperature could possibly due to the merging of the smaller particles into larger particles as per Ostwald ripening.

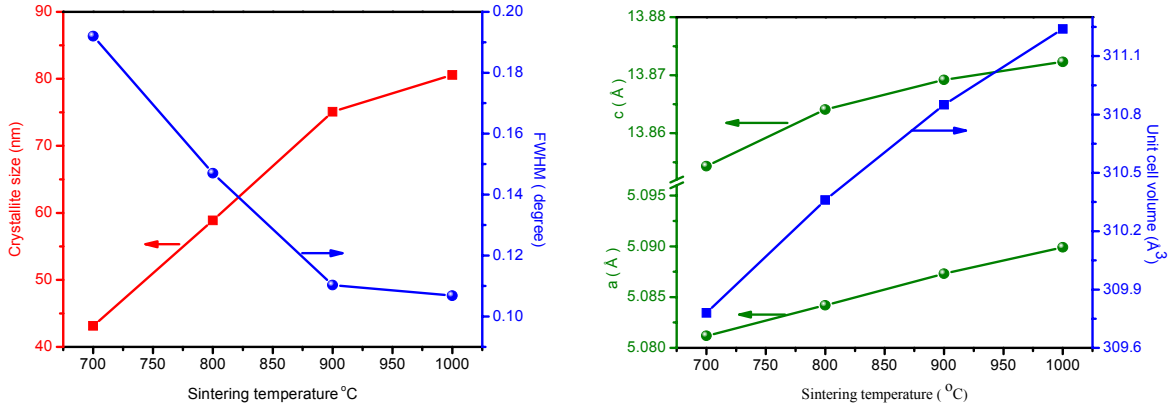

(a) *(b)*

Fig. 2. (a) Variation of crystallite size and FWHM with sintering temperature; (b) Variation of lattice parameter and unit cell volume of $ZnTiO_3$ hexagonal phase with sintering temperature.

Fig. 3 (a-d) shows the FE-SEM images of $ZnTiO_3$ samples sintered at different temperature. The grains are nearly spherical in shape and grain size increases as the sintering temperature increases. Their average diameter is about between 211 nm to 766 nm for different sintering temperature upto 1000 °C. In addition, energy dispersive analysis of x-ray (EDAX) was used to determine ratio of Zn and Ti elements for all samples. The result reveals that the molar ratio of Zn to Ti was found to almost in 1:1 ratio.

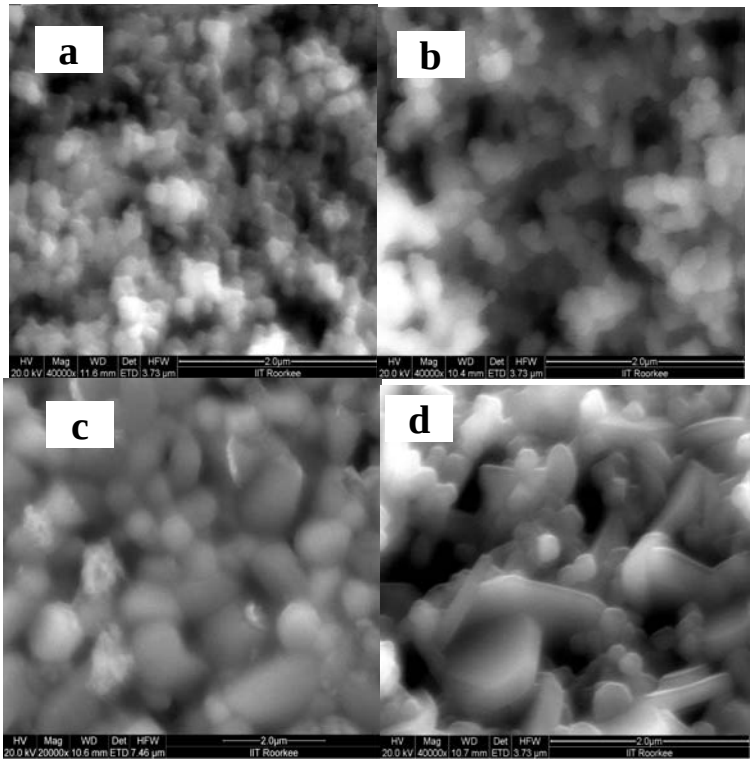

Fig. 3. FE-SEM images of samples sintered at different temperature (a) 700, (b) 800, (c) 900, (d) 1000 °C.

Fig. 4 shows the EDAX curve for ZTO sintered at 800 ^{o}C.

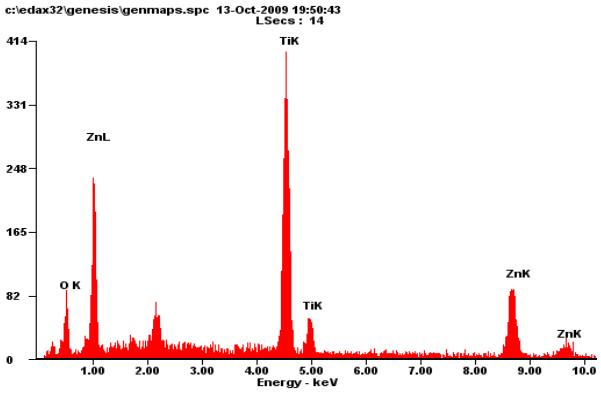

Element	Wt%	At%
OK	28.10	57.63
TiK	30.04	21.77
ZnK	41.86	20.60

Fig. 4. EDAX analysis of ZTO sintered at 800 ^{o}C.

The optical absorption spectra of ZTO for different sintering temperature are shown in Fig. 5. It can be seen in figure that the ultraviolet absorption edge of single hexagonal-phase $ZnTiO_3$ has a red-shift, compared with that of cubic/hexagonal mixed phase $ZnTiO_3$. The absorption edge of particles corresponds to that of cubic/hexagonal mixed phase in the wavelength bands is about 425 nm, which is less than that of single hexagonal-phase $ZnTiO_3$ in the wavelength bands about 431 nm (red-shift). This may be caused by the existence of cubic-phase $ZnTiO_3$ which may modify the optical absorption edge.

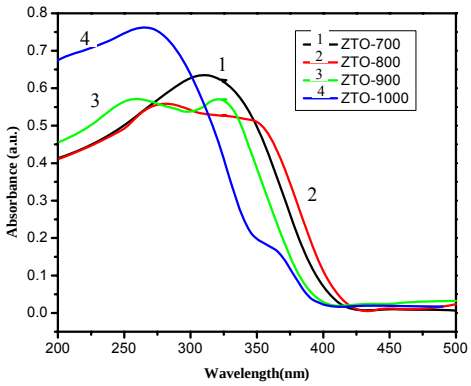

Fig. 5. Absorption spectra of ZTO sintered at different temperature.

For the indirect band-gap semiconductor, the relation between the absorption edge and photon energy ($h\nu$) can be written as follows [31]:

$$\alpha h\nu = A\left(h\nu - E_g\right)^2 \quad (4)$$

where α is the absorption coefficient, A is a constant, h is Planck's constant, ν is the photon frequency and E_g is the optical band gap. The plot of $(\alpha h\nu)^{1/2}$ versus hν of ZTO sintered at different temperature is shown in Fig. 6. An extrapolation of the linear region of a plot of $(\alpha h\nu)^{1/2}$ on the y-axis versus photon energy (hν) on the x-axis gives the value of the optical band gap E_g. The variation of band gap with sintering temperature is shown in inset of Fig. 6.

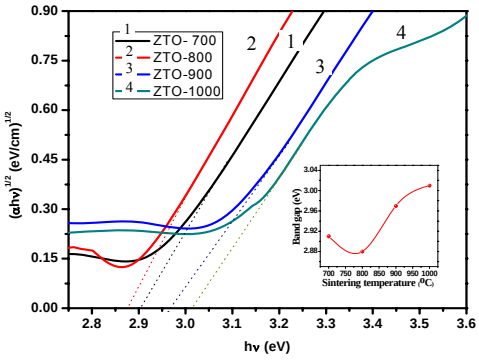

Fig. 6. $(\alpha h\nu)^{1/2}$ versus hν plot of ZTO sintered at different temperature.

It is found that the band gap decreases with the increasing percent of hexagonal-phase upto 800 ^{o}C and when the sintering temperature reaches at 900^{0}C band gap starts to increasing since $ZnTiO_3$ starts to decompose into Zn_2TiO_4 and rutile TiO_2 which has higher band gap than $ZnTiO_3$.

Dielectric constant ε_r is calculated from the measurement of capacitance value which can be obtained using the following equations:

$$\varepsilon_r = \frac{t \times C_p}{A \times \varepsilon_0} = \frac{t \times C_p}{\pi\left(\frac{d}{2}\right)^2 \times \varepsilon_0} \quad (5)$$

$$\tan\delta = \frac{\varepsilon_1}{\varepsilon_r} \quad (6)$$

where, t = thickness of the pellet = 1.15 × 10^{-3} (m), C_p= equivalent parallel capacitance which obtained from the data of measurement, ε_0 = permittivity of vacuum = 8.854 x 10 $^{-12}$ (F/m), d = diameter of electrode = 0.75 x 10 $^{-2}$ (m).

Fig. 7 (a-b) shows the measured capacitance and tangent loss (tan δ) of the samples sintered at various temperatures as a function of frequency in the range 1 kHz to 1 MHz. The plot of calculated relative dielectric constant ε_r versus frequency of the applied field with different sintering temperature is shown in Fig. 8.

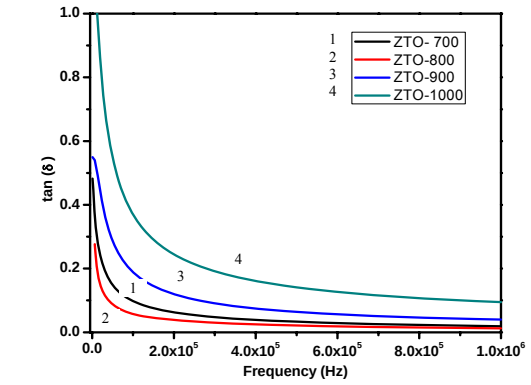

(a)

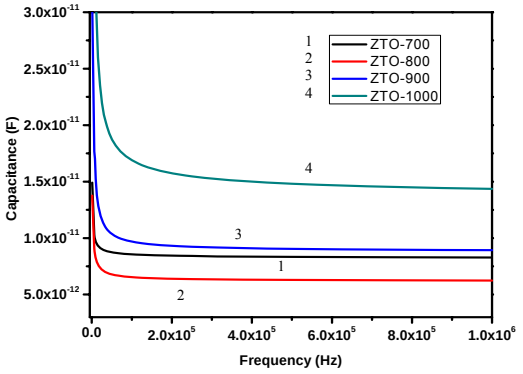

(b)

Fig. 7. (a). Capacitance versus frequency plot for the samples sintered at various temperatures; (b) loss tangent (tan δ) versus of frequency for samples sintered at various temperatures.

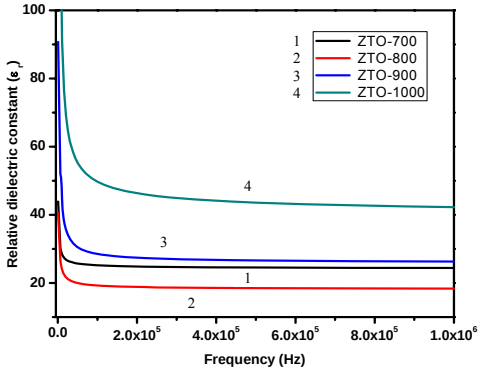

Fig. 8. Relative dielectric constant versus frequency plot for samples sintered at various temperatures.

Based on this, it is seen that the dielectric constant is steeply decreasing in the lower frequency region and has an almost constant value at the higher frequency region. The dielectric loss tangent followed the similar trend. This shows that there is not much frequency dispersion in the dielectric properties for these materials, which is an important property suitable for many applications. At frequencies below 10 kHz the dielectric constant is found to be high and this is attributed to the contribution from the grain boundaries. But for the frequencies above this the dielectric constant depends on the combined effect of both grain and grain boundaries and can be estimated as [32]:

$$\varepsilon = \frac{\varepsilon_b \varepsilon_{gb}}{\varepsilon_b + \varepsilon_{gb}} \quad (7)$$

where ε_b is the bulk permittivity and ε_{gb} is the permittivity from the grain boundaries. Since $\varepsilon_{gb} > \varepsilon_b$ in the higher frequency region we can approximate $\varepsilon \approx \varepsilon_b$. So it is concluded that at higher frequencies only the grains contribute to the dielectric constant of these materials and the grain boundary effects can be neglected.

As the sintering temperature increases from 700 ^oC to 800 ^oC, slight decrease in dielectric constant was observed that could be due to cubic to hexagonal phase transformation. With further increase in sintering temperature i.e. from 900 ^oC to 1000 ^oC dielectric constant was also found to increase, which support the existence of rutile TiO_2 because rutile phase exhibit higher dielectric constant (ε_r~105) compared to hexagonal $ZnTiO_3$ and cubic Zn_2TiO_4 phases [33].

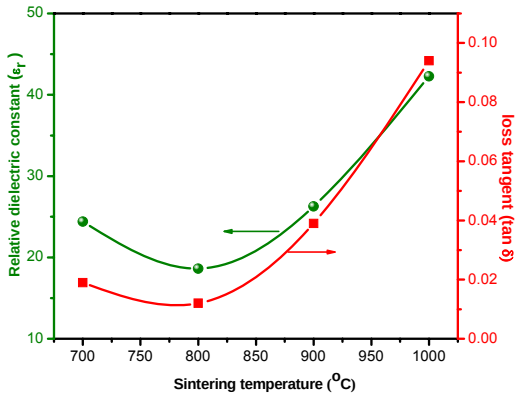

Fig. 9. Room temperature relative dielectric constant and loss tangent of ZTO as a function of sintering temperature (at 1 MHz).

Furthermore, the uniform and well-grown morphology with sintering at 900 °C seems to assist the improvement in dielectric properties. The relative dielectric constant and loss tangent of ZTO as a function of sintering temperature (at 1 MHz) are shown in Fig. 9.

4. Conclusions

A systematic study of $ZnTiO_3$ ceramics leads to the following conclusions: -

1. At 700 ^oC sintering temperature cubic and hexagonal phase of $ZnTiO_3$ appear and single phase

$ZnTiO_3$ appear at 800 ^oC. Further increase in sintering temperature leads to decomposition of $ZnTiO_3$ into Zn_2TiO_4 and rutile TiO_2.

2. We have observed a linear increase in lattice parameters with sintering temperature along with increase in the size of grains. The size increment of the particles with sintering temperature was explained in terms of Ostwald ripening.

3. The optical studies showed that the band gap decreases as the percentage of hexagonal phase of $ZnTiO_3$ increases. The band gap is minimum for single hexagonal $ZnTiO_3$ phase (2.88 eV) as compared to mixed cubic/hexagonal phase (2.91 eV).

4**.** Dielectric constant ε_r and loss tangent (tan δ) sharply decreases with increasing frequency upto 100 kHz and then become frequency independent. The dielectric constant and loss tangent for pure hexagonal phase of $ZnTiO_3$ was found $\varepsilon_r \approx 19$ and tan $\delta \approx 0.01$, respectively, which is suitable for application in microwave resonators, filters etc.

References

[1] P. Singh, A. Kumar, Deepak, D. Kaur, Optical Materials **30**, 1316 (2008).

[2] W. Gao, Z. Li, Ceramics International **30**, 1155, (2004).

[3] P. Singh, A. Kumar, D. Kaur, Physica B: Condensed Matter **403**, 3769 (2008).

[4] M. R. Vaezi, Journal of Materials Processing Technology **205**,332 (2008)

[5] N. Wang, X. Li, Y. Wang, Y. Hou, X. Zou, G. Chen, Materials Letters **62**,3691 (2008).

[6] L. Irimpan, B. Krishnan, V.P.N. Nampoori, P. Radhakrishnan, Journal of Colloid and Interface Science **324**, 99, (2008).

[7] B. B. Rao, Material Chemistry and Physics **64**, 62 (2000).

[8] Y. Yoshino, T. Makino, Y. Katayama, T. Hata, Vaccume **59**, 538 (2000).

[9] S. Jagar, B. Szyszka, G. Brauer, Surface Coating Technology **98**, 1304 (1998).

[10] R. W. Birkmire, E. Eser, Material Science **27**, 625 (1997).

[11] D. C. Look, Material Science Engginering B **80**, 383 (2001).

[12] J. M. Jung, M. Wang, E. J. Kim, S. H. Hahn, Vaccum **82**,872 (2008)

[13] A. B. Bodade, A. M. Bende, G. N. Chaudhari, Vaccum **82**, 588 (2008).

[14] X. Zhang, F. Zhang, K. Y. Chan, Material Chemistry Physics **97**, 384 (2006).

[15] N. Wang, X. Y. Li, Y. X. Wang, Y. Hou, G. H. Chen, Material Letter **62**, 3691 (2008).

[16] L. X. Shi, H. Shen, L. Y. Jiang, X. Y. Li, Material Letter **61**, 4735 (2007).

[17] H. T. Kim, S. Nahm, J. D. Byun, Journal of American Ceramic Society **82**, 3476 (1999).

[18] H. Obayashi, Y. Sakurai, T. Gejo, Journal of Solid State Chemistry **17**, 299 (1976).

[19] Y. Shimizu, Sensors and Actuators B **34**, 493 (1996).

[20] S. F. Wang, M. K. Lu, G. J. Zhou, Inorganic Chemistry Communication **6**, 185 (2003).

[21] M. Skoglundh, Applied Catalyst **53**, 56 (1970).

[22] Y. S. Chang, Y. H. Chang, G. J. Chen, Solid State Communications **128**, 203 (2003).

[23] Y. Gui, S. Li, J. Xu, Microelectronics Journal **39**, 1120 (2008).

[24] S. F. Wang, F. Gu, M. K. Lu, D. R. Yuan, Chemistry Physics Letter **373**, 223 (2003).

[25] F. H. Dulin, D. E. Rase, Journal of American Ceramic Society **43**, 125 (1960).

[26] U. Steinike, B. Wallis, Crystal Research Technology **32**, 187 (1997).

[27] Y. S. Chang, Y. H. Chang, I. Chen, Y. L. Chai, Journal of Ceramic International **30**, 2183 (2004)

[28] L. Hou, Y. D. Hou, M. K. Zhu, J. Tang, J. Liu, H. Yan, Material Letter **59**, 197 (2005).

[29] P. Singh, A. Kumar, Deepak, D. Kaur, Journal of Crystal Growth **306**, 303 (2007).

[30] K. K. Nanda, F. E. Kruis, H. Fissan, Phys. Rev. Lett. **89**, 256103 (2002).

[31] J. Tauc (Ed.), Amorphous and Liquid Semiconductor, Plenium Press, New York.

[32] K. Sudheendran, K C. James Raju, Ceramics International **34**, 897 (2008).

[33] H. T. Kim, J. D. Byun, Y. Kim, Materials Research Bulletin **33**, 963 (1998).

*Corresponding author: dkaurfph@iitr.ernet.in